NJC

Accepted Manuscript

This is an *Accepted Manuscript*, which has been through the Royal Society of Chemistry peer review process and has been accepted for publication.

Accepted Manuscripts are published online shortly after acceptance, before technical editing, formatting and proof reading. Using this free service, authors can make their results available to the community, in citable form, before we publish the edited article. We will replace this *Accepted Manuscript* with the edited and formatted *Advance Article* as soon as it is available.

You can find more information about *Accepted Manuscripts* in the Information for Authors.

Please note that technical editing may introduce minor changes to the text and/or graphics, which may alter content. The journal's standard Terms & Conditions and the Ethical guidelines still apply. In no event shall the Royal Society of Chemistry be held responsible for any errors or omissions in this *Accepted Manuscript* or any consequences arising from the use of any information it contains.

ROYAL SOCIETY OF CHEMISTRY

www.rsc.org/njc

Cite this: DOI: 10.1039/c0xx00000x

www.rsc.org/xxxxxx

ARTICLE TYPE

Novel Ag Deposited Nano Coordination Polymers Derived Porous SnO_2/NiO Heteronanostructure for Enhanced Photocatalytic Reduction of Cr(VI) under Visible Light

Md.Rakibuddin and Rajakumar Ananthakrishnan*

Received (in XXX, XXX) Xth XXXXXXXXX 20XX, Accepted Xth XXXXXXXXX 20XX
DOI: 10.1039/b000000x

Fabrication of a novel porous Ag deposited SnO_2/NiO (Ag/SnO_2/NiO) heteronanostructure for photoreduction of toxic aqueous Cr(VI) to non toxic Cr(III) is reported. The material is prepared by depositing metallic Ag nanoparticle into the SnO_2/NiO heteronanostructure by reduction of Ag^+ under UV irradiation. The SnO_2/NiO heteronanostructure is obtained by facile solid-state transformation of novel nano coordination polymer (NCP) route. The prepared Ag/SnO_2/NiO is characterized by different techniques such as PXRD, XPS, EDX, FESEM, TEM, HRTEM, BET, UV-Vis DRS and PL measurements. The PXRD and XPS studies confirm the formation of Sn(IV) state of the SnO_2 in the heterostructure. TEM images reveal the spherical morphology of Ag nanoparticles with average particle size of 15 nm, and hexagonal shaped SnO_2 and NiO with average particle size of 10 and 5 nm in the Ag/SnO_2/NiO, respectively. The incorporation of Ag enhances visible light absorption and higher electron–hole separation of the Ag/SnO_2/NiO by Surface Plasmon Resonance (SPR). Besides, the material exhibits high surface area and porous nature, which facilitates effective photocatalytic reduction of toxic aqueous Cr(VI) to non toxic Cr(III) under visible light. Furthermore, the photocatalytic reduction of Cr(VI) is optimized under different parameters. The photostability of the Ag/SnO_2/NiO is tested up to five successive runs indicating its promising applications for wastewater treatment. Finally, a photocatalytic mechanism is proposed for the reduction of aqueous Cr(VI) over Ag/SnO_2/NiO under visible light.

Introduction

During the last two decades, energy shortage and environmental deterioration have become the major obstacles to the development of economy and society. The removal of toxic heavy-metal ions (such as Pb(II), As(V), Cr(VI), Hg(II), Cd(II) etc.) from wastewater resources has received significant attention because of their hazardous nature to the environment, and living organisms.[1,2] Among these metals Cr(VI) has been identified as one of the most unsafe metals, which is generated through different industrial processes like electroplating, leather tanning, metal polishing, pigment manufacturing, photography, etc.[3–6] Chromium exists in the environment mainly in two oxidation states, Cr(III) and Cr(VI). Cr(III) is relatively non-toxic and is an essential microelement in the human diet to maintain carbohydrate metabolism and nucleic acid synthesis.[7] On the other hand, Cr(VI) is very toxic in nature due to highly solubility in aquatic systems, and its long-term exposure in drinking water can cause kidney and liver damage, skin cancer, severe diarrhoea, vomiting, and also carcinogenic and mutagenic in living organisms.[8,9] The World Health Organization (WHO) had identified Cr(VI) as a carcinogenic element and allowed limiting concentration as 0.05 mg L^{-1} in drinking water.[10]

Department of Chemistry, Green Environmental Materials & Analytical Chemistry Lab, Indian Institute of Technology, Kharagpur 721302, India. E-mail: raja.iitchem@yahoo.com; Fax: +91 3222-282252; Tel: +91 3222-282322

†Electronic supplementary information (ESI) available: Supporting information is available free of charge via internet at hppt://pubs.rsc.org/.

Therefore, it has become a primary concern to develop effective technologies to reduce Cr(VI) to Cr(III) and remediation of Cr(VI) contaminations for the wastewater treatment and water consumption. Various technologies have been employed for the reduction of Cr(VI) to Cr(III) and its removal, including microbial reduction,[11] photocatalytic reduction,[12,13] and adsorption technique.[14-16] For example, Wu et al. reported photoreduction of Cr(VI) induced by NH_2-mediated zirconium metal organic framework.[17] Song et al. reported the reduction of Cr(VI) in the presence of aqueous medium contained TiO_2 nanosheets under UV−Visible light.[18] Zhang et al. reported visible-light-driven photocatalytic reduction of Cr(VI) in the presence of SnS_2/SnO_2 nanoheterojunction.[19] Among these above-mentioned methods, photocatalytic reduction of Cr(VI) by semiconductor photocatalyst is promising as it is efficient, cost-effective, and does not use or discharge any dangerous chemicals into treated water. To date, several materials have been developed for photocatalytic reduction of Cr(VI) under ultraviolet and visible light irradiation.[20–23]

Metal oxides, such as TiO_2, Co_3O_4, ZnO, NiO and SnO_2 have been the prime choice for basic research and practical applications owing to their high activity, good stability, low cost, non-toxicity and chemical inertness.[24-26] SnO_2 and NiO are significant n-type and p-type semiconductor with band gap of 3.7 eV and 3.6 eV, respectively.[27] These two materials have attracted attention because of their wide range of applications in optoelectronic devices and dye sensitized solar cells, sensors and

water purifications.[28-30] Both the materials normally exhibit high photocatalytic activity under UV light irradiation, however, the visible light photocatalytic activity of the materials is not satisfactory due to their wide band gap absorbing lower amount of visible light. Hence, efficient technique such as loading of noble metals (such as, Pd, Pt, Ag, Au, etc.) into the heterostructures had been employed for harvesting more visible light and enhanced photocatalytic activity by suppressing the recombination of electron and holes.[31,32] The electrons in noble metals are excited by the SPR phenomenon and are transferred to the conduction band of the metal oxide. The transferred electrons move to the surface of the metal oxides and assist the formation of super-oxide radical or the photoreduction process.[33] In addition, it has been found that Ag could be a promising mediator for industrial application compared to other noble metals due to its low cost, non-toxicity, high surface energy with surface defects, unusual electric and optical properties and also for facile fabrication of silver nanoparticles by reduction of Ag^+ using UV irradiation.[34-36] Critically, the work function of silver is much lower than that of other noble metals such as gold and platinum, which favours the formation of good band alignment.[37] Therefore, researcher have tried to synthesize various Ag-based semiconductor composites for photocatalytic application.

Herein, we report the fabrication of a novel porous highly efficient $Ag/SnO_2/NiO$ nanohybrid for the photo-reduction of toxic aqueous Cr(VI). The material is prepared by depositing metallic Ag nanoparticle into the SnO_2/NiO heterostructure by reduction of Ag^+ under UV irradiation. The SnO_2/NiO heteronanostructure is prepared by facile calcinations of a novel NCP precursor. It is worth noting that making hybrid metal oxides from the NCP is now demandable, because this process improves the facile solid-state diffusion and interfacial contact to make a uniform heterojunction at the nanoscale.[38,39] Besides, a porous structure is formed by the decomposition of the organic ligands during calcinations, and also the process is very fast, which occur under mild conditions. Earlier literature reports various methods for the preparation of $NiO\text{-}SnO_2$ composites for applications in gas sensing or as anode materials.[40-44] However, to the best of our knowledge, there is no report on synthesis of SnO_2/NiO in this facile route, and also the heteronanostructure has not been applied for any photocatalytic applications previously. Hence, the novel $Ag/SnO_2/NiO$ is prepared, characterized and applied as a photocatalyst for the effective reduction of hazardous Cr(VI) under visible light.

Experimental

Reagents and materials

Silver nitrate and Tin (II) acetate were obtained from Sigma-Aldrich, and Ni (II) acetate dihydrate was obtained from SISCO Research Laboratories Pvt. Ltd. (India). Terephthalic acid was obtained from Central Drug House (P) Ltd. (India). All other chemicals (solvents) used in this experiment are analytical grade (99.9%). All the solutions were prepared in ultrapure water (Milli-Q system).

Preparation of porous Sn-Ni nano coordination polymer (NCP) and corresponding SnO_2-NiO heteronanostructures

Firstly, Sn-Ni mixed metal NCP was synthesized *via* facile novel nano coordination polymer route.[38,45] Typically, a solution of $Sn(OAc)_2.2H_2O$ (0.028 mmol) and $Ni(OAc)_2.4H_2O$ (0.021 mmol) were dissolved in a 4: 3 ratio in a minimum amount of DMF, and 3 mL DMF solution of 1,4-benzene dicarboxylic acid (H_2BDC) (0.035 mmol) was added to the above prepared solution. Within seconds, mixed-metal NCP began to form. Products were centrifuged and washed with acetonitrile two times. The mixed-metal Sn-Ni NCPs were then dried at open air (yield ~60%). Sn NCP was also prepared for comparison by following similar procedure instead of adding nickel acetate salt.

Finally, the as-prepared mixed-metal [Sn-Ni (BDC)].H_2O NCP or shortly, Sn-Ni NCP were then placed in a conventional furnace and heated at 450 °C for 90 min (see Supporting Information, Scheme 1). The porous SnO_2-NiO heteronanostructures were generated, and cooled to room temperature. The loss of weight from polymer to metal oxides at 450 °C was ~40-50% confirmed by TGA (Figure S1-S4, see supporting information for the details of NCP characterization).

Preparation of $Ag/SnO_2/NiO$ nanohybrid heterostructure

The silver-deposited SnO_2/NiO heteronanostructure was prepared by photocatalytic reduction of $AgNO_3$ (2×10^{-4} M in water) in a suspension containing SnO_2/NiO hybrid (1 g/L) in water. The mixture was irradiated in presence of a 6W Hg UV lamp (λ=352 nm). The colour of the suspension was observed to be changed from pale-brown to light grey indicating the reduction of Ag^+ and the deposition of silver on SnO_2/NiO. The photodeposition is completed within 60 min, which was checked by the procedure described in details elsewhere.[46] The irradiated mixture was centrifuged and then washed by high purity water several times to obtain nitrate free washing water. Finally, the prepared $Ag/SnO_2/NiO$ photocatalyst was dried in an oven at 80 ◦C. The ICP-MS analysis of the hybrid sample showed 5 wt% loading of the silver metal into the heteronanostructure which also agreed well with the EDX measurement.

Visible light photocatalytic reduction of aqueous Cr(VI)

The photocatalytic reduction of the Cr(VI) was evaluated at room temperature taking 30 mL of $K_2Cr_2O_7$ (2×10^{-4} M) solution of an aqueous medium in a Pyrex glass vessel in the presence of various dosages of the catalyst, $Ag/SnO_2/NiO$ (0.25 to 1.0 g/L) at different pH values (2 to 10). The solution was kept in the dark under stirring for 6 h to reach adsorption-desorption equilibrium. After that, the solution was irradiated under visible light (300 W halogen lamp that contained the aqueous $NaNO_2$ solution (10% w/w) as a light filter through which only visible light, λ≥420 nm could pass; incident light intensity 2.98×10^{16} Einstein L^{-1} s^{-1}). After a certain regular interval of irradiation time, a particular amount of the aliquot was taken from the reaction mixture, and the catalyst was separated by centrifugation (5000 rpm for 5 min). The transparent solution thus obtained after centrifuge was preserved in the dark for spectral analysis recorded by UV-1601 SHIMADZU spectrophotometer.

Results and Discussion

Characterization of the SnO_2, SnO_2/NiO and $Ag/SnO_2/NiO$ heteronanostructure

Sn-Ni NCPs are first synthesized by mixing $Sn(OAc)_2$ and

$Ni(OAc)_2$ with BDC ligand in DMF solution. When the DMF solution of $Ni(OAc)_2$ and $Sn(OAc)_2$ are added to the BDC solution in DMF, Sn^{2+} and Ni^{+2} are getting coordinated to occupy the carboxylate node position, and hexagonal lump NCP began to form within minutes. Interestingly, formation of the NCPs does not occur when MCl_2, $M(NO_3)_2$ or $M^{II}SO_4$ are used as metal salts instead of $M(OAc)_2$. The above results prove that the formation of the NCP is highly salt dependent. The as-prepared Sn-Ni NCPs are first characterized by FT-IR, PXRD and TGA study, and then are calcined at 450 ºC for 75 min to obtain SnO_2/NiO heterostructure. The silver metal is then deposited on the SnO_2/NiO heteronanostructure by photocatalytic reduction of $AgNO_3$ in the aqueous suspension of SnO_2/NiO under UV light irradiation. Finally, Ag/SnO_2/NiO ternary hybrid is obtained and characterized.

Figure 1 presents the PXRD patterns of NCP derived pure SnO_2, SnO_2/NiO and Ag/SnO_2/NiO hybrid. The NCP derived pure SnO_2 shows the peaks at 2θ =26.4, 33.7 38.08, 51.8, 54.8, 58.0, 61.8, 65.5, 71.3, 78.6 and 83.7 which correspond to (1 1 0), (1 0 1), (2 0 0), (2 1 1), (2 2 0), (0 0 2), (3 1 0), (1 1 2), (3 0 1), (2 0 2) and (3 2 1) planes, respectively, which are well indexed to the tetragonal rutile structure of SnO_2 nanoparticles (JCPDS 41-1445).[47] In the SnO_2/NiO sample, along with the SnO_2 peak, the peaks at 2θ =37.2, 43.0, 62.5, 75.5, 78.4 correspond to (111), (200), (220), (311) and (222) plane of pure cubic NiO, respectively (JCPDS, 4-0835).[48] In addition with the peak of SnO_2 and NiO, the peaks at 2θ = 38.2, 44.2, 64.6 and 77.5° correspond to (1 1 1), (2 0 0), (2 2 0), (3 1 1) planes of face-centered-cubic (fcc) lattice of metallic Ag[49] (JCPDS file no. 04-0783) in the Ag/SnO_2/NiO sample. However, the peak of NiO in the Ag/SnO_2/NiO hybrid is found to be less intense indicating higher crystalline nature of the NiO in the hybrid. There is no remarkable shift of other diffraction peaks, and no other crystalline impurities are observed indicating the high purity of the sample.

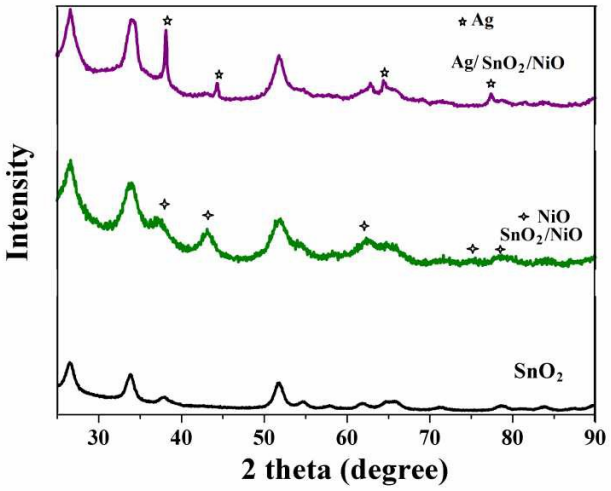

Fig. 1 Powder X-ray diffraction patterns of synthesized SnO_2, SnO_2/NiO and Ag/SnO_2/NiO hybrid.

The visible light absorption properties of pure SnO_2, SnO_2/NiO and Ag/SnO_2/NiO are examined by UV-visible diffuse reflectance spectra (DRS) (Figure 2). The UV-Vis absorbance spectrum of SnO_2 shows absorbance maxima (310 nm) in the UV range because of their wide band gap. Compared with pure SnO_2, a broad extended absorbance is observed of the Ag/SnO_2/NiO in the visible region due to the SPR absorption of metallic Ag nanoparticles, which is expected to improve the photocatalytic activity under visible light irradiation. It is worth noting that the UV-Vis DRS spectra of the SnO_2/NiO heterostructure also shows absorption in the whole visible region due to its blackish colour, but it exhibits very poor visible light photocatalytic activity due to higher rate of recombination of charge carriers.

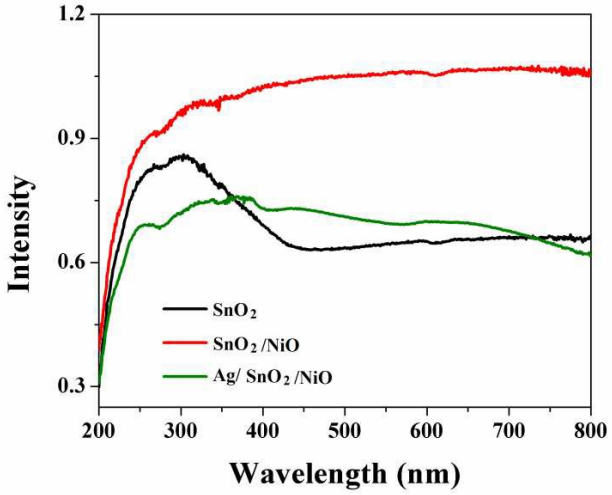

Fig. 2 Diffuse reflectance spectra of synthesized SnO_2, SnO_2/NiO and Ag/SnO_2/NiO hybrid.

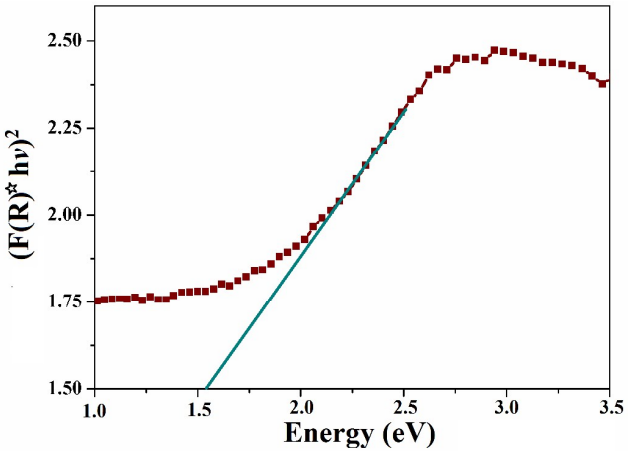

Fig. 3 Plot of $[F(R) hv]^2$ versus photon energy (hv) for determination of band gap of the as-synthesized Ag/SnO_2/NiO hybrid.

,

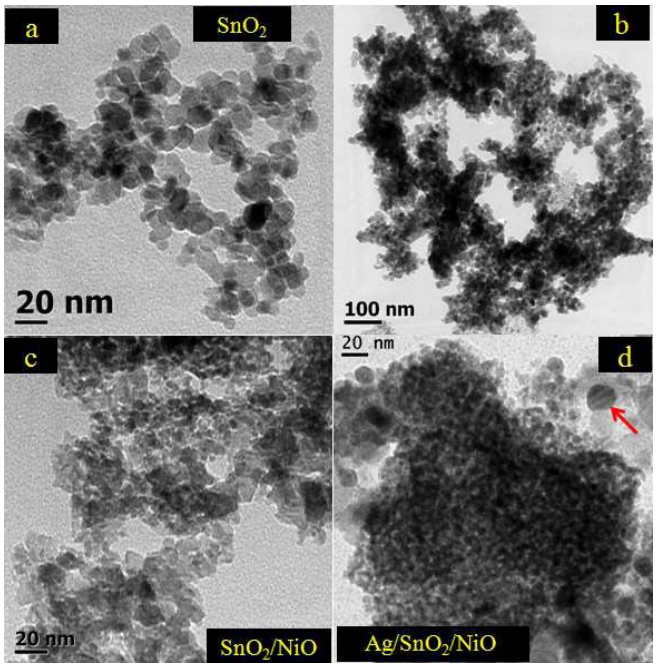

Fig. 4 TEM images of a) SnO_2, b-c) SnO_2/NiO and d) Ag/SnO_2/NiO hybrid.

Furthermore, it is known that for a direct semiconductor the optical absorption near the band edge obeys the equation: $\alpha(h\nu) = A(h\nu - E_g)^{1/2}$ where α, ν, E_g, and A are the absorption coefficient, light frequency, band gap energy, and a constant, respectively. The absorption coefficient (α) can be replaced by the remission function, F(R) and can be written in terms of diffused reflectance (R) according to the Kubelka−Munk theory as, α/s =F(R) = $(1- R)^2/(2R)$, where s is the scattering coefficient. The band gap energies (E_g values) of the samples can then be obtained by the intercepts of the tangents of the plot $[F(R)\ h\nu]^2$ *vs.* f(hν) (Fig. 3). For the pure SnO_2 and Ag/SnO_2/NiO hybrid, the band gaps are estimated to be 3.67 eV (Fig. S5) and 1.51 eV, respectively.

In order to obtain detailed information about the nanostructure and morphology of as-synthesized samples, TEM, FESEM and HRTEM studies are carried out. Figure 4 shows TEM images of the pure SnO_2 nanoparticle distributed within particle size range 7-15 nm, and having a nearly hexagonal shape with average particle size of 10 nm. The Figure 4b and 4c show low and high magnification images of the SnO_2/NiO having both SnO_2 and NiO in the sample, where the average size of the SnO_2 and NiO is 10 nm and 5 nm, respectively, which is lower than corresponding porous Sn-Ni NCP precursor (Figure S4). As the TEM images exhibit the presence of both nanoparticles SnO_2 and NiO, hence, resulting sample is heteronanostructure rather than nanocomposite. Because in nanocomposites, two or more components interact each other to form a single component and the two components cannot be identified separately; however, in heteronanostructure, there is an interface between two solid-state materials and the two components can be distinguished separately. The Figure 4d shows the TEM images of the Ag/SnO_2/NiO hybrid, where some new spherical Ag nanoparticles with average particle size of 15 nm are attached to the surface of the SnO_2/NiO heteronanostructure (also see Figure S6).

Moreover, Ag aggregates are not found in the TEM observations, indicating that all metallic Ag nanoparticles are completely dispersed in Ag/SnO_2/NiO. Furthermore, in Figure 5a, the HR-TEM image of the pure SnO_2 nanoparticles clearly reveals the lattice fringes with interplanar spacing of 0.34 nm, which is assigned to the (110) plane of SnO_2.[30] The lattice fringes with spacing of 0.243 nm are observed for NiO in the SnO_2/NiO sample assigned to (111) plane of cubic NiO (Figure 5b).[50] Again, the HR-TEM image (Figure 5c) taken from the interface part of the Ag/SnO_2/NiO hybrid clearly displays the presence of SnO_2, Ag and NiO of different contrasts indicated by the lattice fringes with interplanar spacing of 0.236 nm for (111) planes of the Ag[51], 0.34 nm for the (110) plane of SnO_2 and 0.243 nm for the (111) plane of NiO. SAED patterns (in Fig.5d-g) confirms the single crystalline nature of all the materials, which is also good agreement with the HRTEM results.

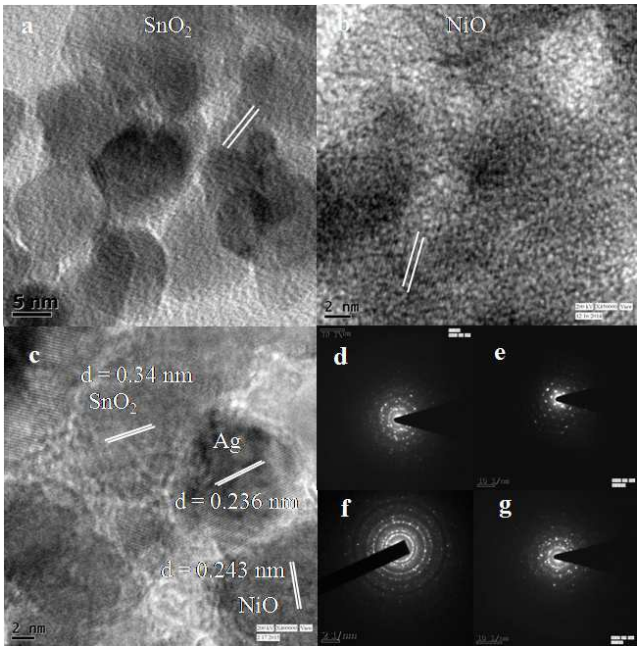

Fig. 5 HRTEM images of a) SnO_2, b) NiO in the SnO_2/NiO, c) Ag/SnO_2/NiO nanohybrids, and d-g) SAED pattern of the respective samples.

The morphology and size of nanoparticles are also in well agreement with the FESEM images of the samples (Figure 6a). The EDX spectrum is obtained during TEM analysis of the Ag/SnO_2/NiO further confirms only the presence of Sn, Ag, Ni and O in the samples, and the absence of any other impurities (Figure 6b). The peak of C and Cu are obtained due to carbon coated Cu grid used for sample preparation in TEM analysis (Figure S7). The Figure 6d-g shows the elemental mapping of the Sn, Ag, O and Ni in the selected area of the FESEM image of Ag/SnO_2/NiO in Figure 6c.

The elemental area mapping of the materials also indicates successful incorporation of the elements in proper proportions into the heteronanostructures. Hence, EDX, elemental mapping and the XRD results of the sample are in good agreement with each other.

XPS measurements have been further conducted to study the

surface composition and valence states of the elements existing in the final products. The XPS surveys of $Ag/SnO_2/NiO$ (Figure 7a) revealed that only Sn, Ni, Ag and O elements existed in the samples and no trace of any impurity is observed. The high-resolution XP spectra of the Sn 3d exhibits two major peaks at 486.7 and 495.8 corresponding to the binding energy of Sn(IV) of the SnO_2 (Figure 7b) in the $Ag/SnO_2/NiO$ hybrid.[52]

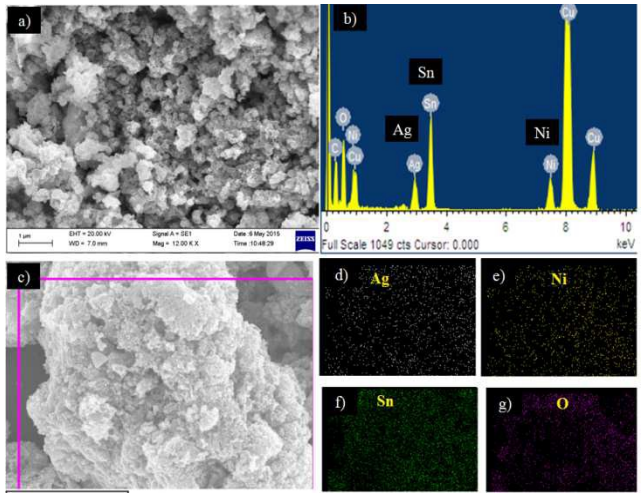

Fig. 6 a) FESEM image, b) EDX profiles and d-g) Elemental mapping analysis of the synthesized $Ag/SnO_2/NiO$ hybrid.

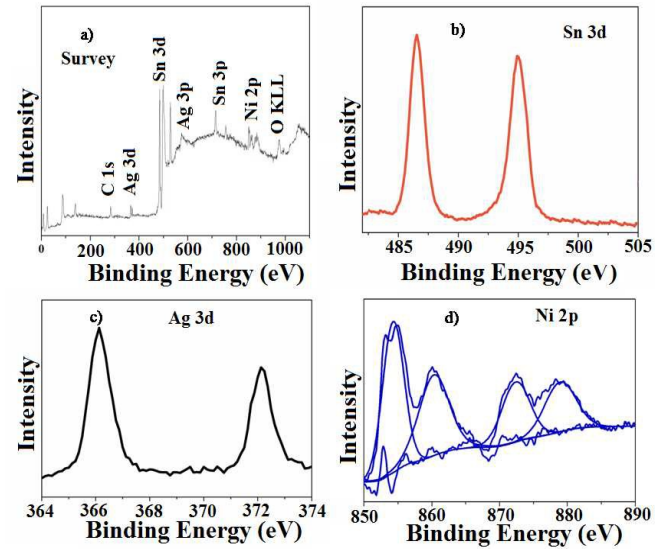

Fig. 7 a) XPS full survey of the synthesized $Ag/SnO_2/NiO$ hybrid, b) High resolution XPS measurement of the Sn 3d, c) Ag 3d and d) Ni 2p of the hybrid.

Hence, XPS of the Sn 3d infers that the Sn exists as Sn(IV) (SnO_2) in the sample, and no trace amount of metallic Sn(0) is observed during photo reduction of Ag^+ ions. Figure 7c shows the XPS of Ag 3d in the sample. The peaks locating at 366.1 and 372.1 eV are attributed to Ag $3d_{5/2}$ and Ag $3d_{3/2}$, respectively confirming the presence of metallic Ag (Ag^0)[53] and the difference in binding energy of 6.0 eV is also characteristic of metallic Ag confirming the photoreduction of Ag^+ ions. The binding energy peaks of Ag 3d in the sample shifts downward compared with pure metallic Ag (367.5 eV) due to the strong interaction between Ag and SnO_2/NiO.[30] The high resolution XPS of Ni 2p shows two major peaks centred at 872.5 and 854.3 eV are indexed to the Ni $2p_{1/2}$ and Ni $2p_{3/2}$, respectively of the NiO, and the satellite peaks at 879.2 and 860.4 eV are two shake-up peaks of the NiO (Figure 7d).[54,55] The high resolution XPS fitting peak of O 1s shows two peaks. The first one appeared at the binding energy of 528.4 eV, which is due to a typical metal–oxygen bond of SnO_2/NiO (Figure S8), and another one appears at 531.0 eV is indicative of hydroxyl groups adsorbed on SnO_2 or NiO surface.[56]

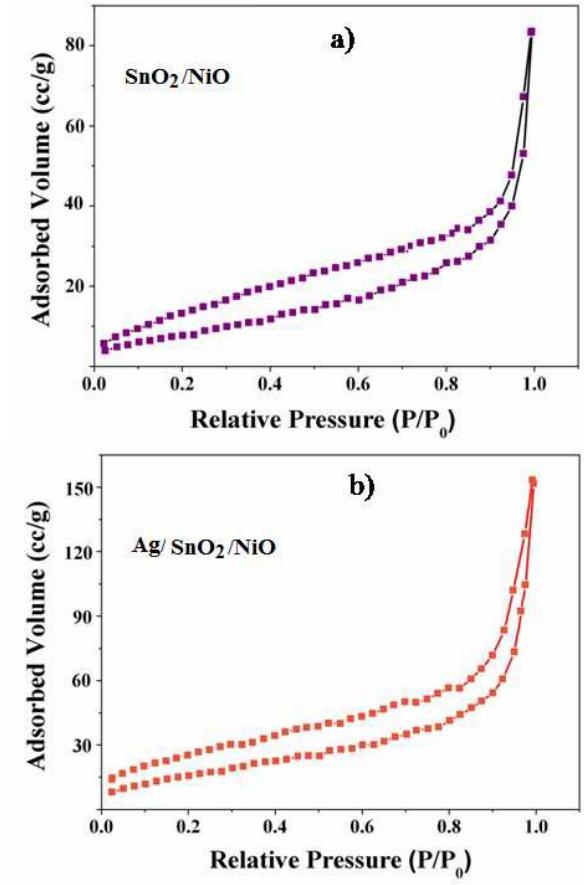

Fig. 8 BET-N_2 gas sorption isotherm curves of a) SnO_2/NiO and b) $Ag/SnO_2/NiO$ hybrid.

The porosity and surface area of the SnO_2/NiO and $Ag/SnO_2/NiO$ are characterized by Brunauer–Emmett–Teller (BET) nitrogen adsorption–desorption isotherm measurements (Figure 8). As shown in Figure 7, the BET isotherms of the prepared materials follow type III behavior indicating weak van der Waals force of attraction between the adsorbate (N_2 gas) and adsorbents (heteronanostructures). Thus, the isotherms are reversible in nature as soon as the pressure is released and hence, explain the multilayer sorption property of the materials.[57] The BET specific surface area and pore volume of $Ag/SnO_2/NiO$ is significantly higher (170.2 m^2/g and 0.422 cc/g, respectively) than that of the SnO_2/NiO (110.4 m^2g^{-1} and 0.367 cc/g, respectively). The surface area of the bare SnO_2 is also measured, which is found to be lower (90 m^2g^{-1}) than the SnO_2/NiO. However, the obtained SnO_2

from the NCP route possessed comparatively higher surface areas than other methods. The high specific surface area and porosity of the $Ag/SnO_2/NiO$ could be attributed to the adsorption of metallic Ag nanoparticles on the SnO_2/NiO surface. Hence, the higher surface area and porous structure of $Ag/SnO_2/NiO$ could promote higher photocatalytic activity by adsorbing more reactant molecules on the catalyst surface.

The optical properties of the synthesized heteronanostructures are examined by Photoluminescence (PL) spectroscopy. Figure 9 shows the PL spectra of pure SnO_2, SnO_2/NiO and $Ag/SnO_2/NiO$. It is established that electron–hole recombination rate is directly related to the intensity of the PL spectrum. Hence, higher rate of electron–hole recombination gives more intense the spectrum. Similarly, a low intensity spectrum in the PL indicates more number of excited electrons are trapped and transferred stably through the interface.[58] It is observed that pure SnO_2 exhibits the strongest emission intensity in the PL spectrum, confirming the higher rate of charge recombination. Interestingly, the PL intensity for the SnO_2/NiO is reduced significantly and this reduction in intensity is more significant for the $Ag/SnO_2/NiO$. This result indicates successful deposition of metallic Ag into the SnO_2/NiO, which can trap photo-generated electrons effectively and inhibits the electron–hole recombination. The effective charge separation facilitates the material to serve as a prominent visible light photocatalyst.

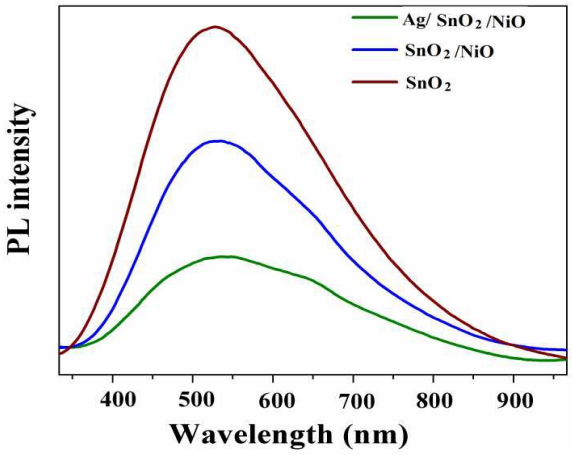

Fig. 9 Photoluminescence spectra of the synthesized SnO_2, SnO_2/NiO and $Ag/SnO_2/NiO$ hybrid.

Photocatalytic reduction of aqueous Cr(VI)

As Cr(VI) is highly hazardous to living organisms, it should be rapidly eliminated before it is discharged into the environment. Here, the photocatalytic reduction of aqueous Cr(VI) (2×10^{-4} M) is performed in presence of various dosages of the $Ag/SnO_2/NiO$ catalyst (0.25-1.0 g/L) at various pH values (2-10) under visible light irradiation. The as prepared $Ag/SnO_2/NiO$ have good surface area, large pore volume and photochemical activities, which makes a perfect visible light photocatalyst for the reduction of Cr(VI) into Cr(III). Figure 10 shows the photocatalytic reduction of aqueous Cr(VI) under visible light irradiation in the presence of the as-synthesized $Ag/SnO_2/NiO$. The UV-Visible absorption spectra for photocatalytic reduction of aqueous Cr(VI) shows (Figure 10a) that the main absorption band of Cr(VI) centred at 365 nm, which notably decreases with the exposure time. The result is also in agreement with the gradual colour change of the solution from yellow to laurel-green with irradiation time.

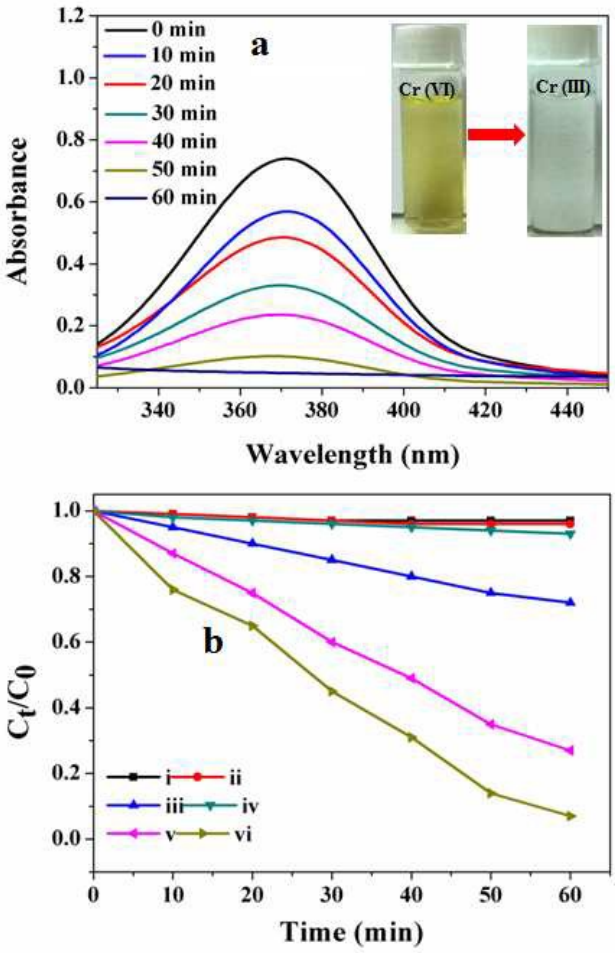

Fig. 10 a) UV- Visible absorption spectra for the reduction of Cr(VI) in presence of the $Ag/SnO_2/NiO$ hybrid ([Cr(VI)]=20 mg/L, [catalyst]= 1.0 g/L, pH=2.0), b) Kinetic plots (C_t/C_0 vs Time) and control studies for the visible light ($\lambda \geq 420$ nm) photocatalytic reduction of Cr(VI) in the presence of i) $Ag/SnO_2/NiO$ under dark, ii) without catalyst under visible light, iii) only SnO_2/NiO under visible light, iv) only SnO_2 under visible light, v) in presence of Ag/SnO_2 under light, and vi) $Ag/SnO_2/NiO$ hybrid ([catalyst]= 1.0 g/L, pH= 2.0, [Cr(VI)]= (2×10^{-4} M).

The photocatalytic reduction of Cr(VI) by various metal oxide/composite photocatalysts reported in literature are summarized in Table 1. There are many limitations observed in the reported studies[59-66] including UV light is utilized as irradiation source or the rate and the duration of photoreduction process is prolonged. However, the as-prepared $Ag/SnO_2/NiO$ inherits remarkable photochemical reducing capability, and $Cr_2O_7^{2-}$ ions are almost completely (98%) reduced within 60 min of irradiation with rate constant of 2.3×10^{-2} min^{-1}. Here, the rate of the reaction, efficiency of the catalyst and utilization of visible light (with moderate power) are noteworthy. Interestingly, the $Ag/SnO_2/NiO$ exhibited an enhancement in photocatalytic reduction of Cr(VI) compared to Ag/SnO_2 synthesized by a similar procedure applied to the former without adding Ni^{+2} salt during preparation.

Table. 1 Comparison of photocatalytic reduction of Cr(VI) by various metal oxide hybrids under UV and visible (Vis.) light conditions

Catalyst	Conditions	Removal	k, min^{-1}	References
ZnO	125 W UV, Cat.:1 g/L [M]:15 mg/L	78% 120 min	0.007	**59**
ZnO–RGO composite	500 W UV, Cat.:1 g/L [M]:10 mg/L	98% 250 min	-	***60***
POM/ TiO_2 nanofibers	300 W UV, Cat.:0.5 g/L [M]: 80 mg/L	65 - 90% 60 min	-	***61***
SnS_2/SnO_2	500 W Vis., Cat.: 1 g/L [M]:10 mg/L	>99.7% 30 min	-	***62***
Hematite/ Activated GO	300 W Vis., pH 2, Cat.:1 g/L [M]:15 mg/L	>95% 160 min	0.018	***63***
CuO–ZnO	300 W Vis., Cat.: foil [M]:10 mg/L	100% 80 min	-	***64***
$SiO_2/NiTiO_3$	200W Vis., Cat: 1 g/L [dye]: 2 mg/L	90% 150 min	-	***65***
Ag/titanate	UV light Cat: membrane [Methamidophos] -----	87% in 30 min	-	***66***
Ag deposited SnO_2–NiO	300 W Vis., Cat.:1 g/L [M]:20 mg/L	98% 60 min	0.023	***This study***

Cat. = amount of catalyst and [M]= concentration of Cr(VI).

The prepared Ag/SnO_2 showed ~75% photocatalytic reduction of Cr(VI) in 60 min of visible irradiation. When the photoreduction of Cr(VI) is carried out in presence of bare SnO_2 and SnO_2/NiO individually under visible light, only 6% and 27% photoreduction of Cr(VI) is observed in 60 min, respectively with rate constant of 1.2×10^{-3} and 5.1×10^{-3} min^{-1} (Figure S9). Though the PL spectra showed the electron–hole separation is improved for SnO_2/NiO, it could not exhibit high photocatalytic activity due to lower absorption of visible light for its wide band gap. A control study (Figure 10b) is carried out in the presence of the catalyst without visible light exposure, but no significant change of Cr(VI) concentration is noticed. Hence, this result infers that the removal of aqueous Cr(VI) is entirely photocatalyst-driven reduction of Cr(VI), rather than a simple physical adsorption of Cr(VI). Again, when an experiment was conducted in the absence of a catalyst under visible light irradiation, there was no significant change in the concentration of Cr(VI) observed. This indicates that the direct photolysis could not drive the reduction of Cr(VI) under visible light irradiation. The dark adsorption study shows that the concentration of the Cr(VI) is decreased to ~20% after 120 min of stirring in dark in presence of the Ag/SnO_2/NiO catalyst, and then it comes to an equilibrium (Fig. S10a). Hence, before the light irradiation, the Cr(VI) solution (20 mg/L) is stirred under dark condition up to 2.5 h in presence of the catalyst each time. It is observed that the apparent rate constant (k_{app} = 1.6×10^{-3} min^{-1}) in the dark condition (Fig.S10b) is much lower than the rate of Cr(VI) reduction under the visible light in presence of the same Ag/SnO_2/NiO catalyst. Overwhelmingly, the photoreduction by SnO_2/NiO (27%) and Ag/SnO_2 (~75%) is lower than that of the hybrid, Ag/SnO_2/NiO (98%) for the 60 min irradiation by the visible light. Hence, it is clear the extent of photoreduction is not only depending on the effective charge separation but also interfacial transportation of photogenerated carriers across the system[62]. The Ag/SnO_2/NiO hybrid offered superior efficacy in the photoreduction due to effective visible light absorption, optimum separation of charges through interfacial transfer of carriers, and capability in decreasing recombination process.

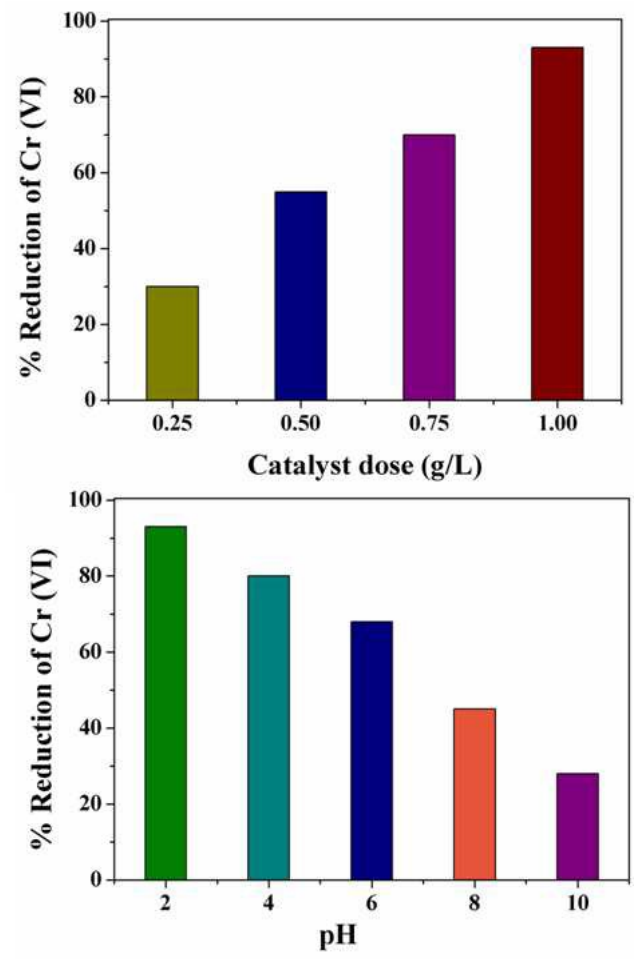

Fig. 11 Effect of a) catalyst loading and b) pH of the solution for the reduction.of aqueous Cr(VI) in presence of Ag/SnO_2/NiO: Experimental conditions: [catalyst =0.25-1.75 g/L, pH= 2-9, [Cr(VI)]=20 mg/L].

Effect of catalyst dose and initial pH for the photo-reduction of aqueous Cr(VI)

Figure 11a shows the photo reduction of Cr(VI) under various catalyst dosages from 0.25 to 1 g/L. It is observed that with the

increase in catalyst dosage, the rate of photocatalytic reduction increases (Figure S11). This is due to the fact that with the increase in catalyst dosage increases the number of plasmonic Ag nanoparticles, which tend to absorb more visible light. Consequently, more photoexcited electrons are generated due to better electron-hole separation, which facilitates the photocatalytic reduction of Cr(VI) to Cr(III).[67]

The effect of pH on the visible light-driven photocatalytic reduction of Cr(VI) in the presence of $Ag/SnO_2/NiO$ is examined by varying the pH from 2.0 to 10.0, at a constant photocatalyst dosage 1g/L. As depicted in Figure 11b, the photo reduction of Cr(VI) slowed down with increased pH. It is observed that the photocatalytic reduction of Cr(VI) in low pH condition is much higher than higher pH condition (Figure S12). At low pH, Cr species exists as $HCrO_4^-$, as the pH increases it become $Cr_2O_7^{2-}$. Therefore, at low pH, the surface of the photocatalyst becomes highly protonated for better accumulation of $HCrO_4^-$ ions. At higher pH, the surface of the photocatalyst becomes negative, which tends to repel the $Cr_2O_7^{2-}$ ion and hence decreases its photocatalytic activity.[68] Besides, at higher pH, the deposition of $Cr(OH)_3$ on the surface of photocatalyst also causes a decrease in photocatalytic activity.[69]

The reusability of the photocatalysts has always been vital for its industrial application, and therefore, it is crucial to study the stability of the as-synthesized $Ag/SnO_2/NiO$ in photocatalytic reduction of aqueous Cr(VI). The stability of the as-prepared photocatalysts is examined by monitoring the photocatalytic activity after five successive cycles of operations (Figure 12). The results reveal that the photocatalytic activity of the catalyst towards reduction of $Cr_2O_7^{2-}$ ions decreased very slightly after each cycle, and it decreased up to 9% after fifth cycles of operation. The slight decrease of the activity may be attributed to the deposition of small amounts of Cr(III) after each cycle.[69]

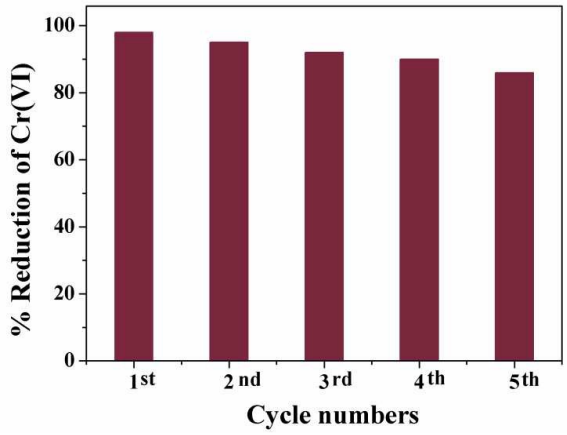

Fig. 12 Reusability of the $Ag/SnO_2/NiO$ catalyst for the reduction. of Cr(VI).

After each cycle, the photocatalyst is separated by centrifugation and washed with dilute HNO_3 solution to diminish the greenish $Cr(OH)_3$ deposited on the surface of the catalyst, and dried under vacuum for further use. The PXRD and SEM image of the catalyst after photocatalytic reduction show no change in PXRD pattern and the presence of spherical Ag metal is still observed (Figure S13). Hence, It infers that the synthesized $Ag/SnO_2/NiO$ hybrid possessed high stability and did not photocorrode significantly during the photocatalytic reduction of Cr(VI), which shows its potentiality in its promising applications for wastewater treatment.

Mechanism of photocatalytic reduction of aqueous Cr(VI)

The Cr(VI) at low concentration mainly exists as H_2CrO_4 and $HCrO_4^-$ forms, whereas at high concentration Cr(VI) exists in $Cr_2O_7^{2-}$ form. However, in acidic medium, $HCrO_4^-$ is the predominant form, whereas CrO_4^{2-} is found in a neutral or basic medium of Cr(VI). The equilibrium of Cr(VI) in solution can be expressed as follows.[70,71]

$$H_2CrO_4 \longrightarrow HCrO_4^- + H^+ \quad pK_a = 1.2$$
$$HCrO_4^- \longrightarrow CrO_4^{2-} + H^+ \quad pK_a = 6.52$$

When $Ag/SnO_2/NiO$ hybrid photocatalyst is exposed to visible light irradiation, the electrons in Ag metals are excited by the SPR phenomenon and are transferred to the conduction band (CB) of the NiO (-0.1 eV)[72] creating holes in the valence band of Ag metal (Figure 13). The transferred electrons in the NiO further moved into the CB of SnO_2 (0.07 eV)[51] as the conduction band edge of the SnO_2 lies below the NiO, whereas the valence bad (VB) potentials of the NiO (3.58 eV)[72] lies above the VB of SnO_2 (3.67 eV).[51] The stepwise interfacial transportation of photogenerated electron is an important step assumed in our system helpful to decrease the recombination process. At the conduction band of SnO_2, the photoexcited electrons (e^-) are utilized for reduction of Cr(VI) to Cr(III), while at the same time the holes (h^+) in the metallic Ag nanoparticles oxidize water molecules to O_2 in its valence band.

As photoreduction of Cr(VI) has been carried out at low concentration, there is great possibility for the Cr to be present in its $HCrO_4^-$ form. The proposed reaction pathway for the photocatalytic reduction of Cr(VI) over $Ag/SnO_2/NiO$ in aqueous solution at pH 2.0 under visible light can be described by the following equations :

$$Ag/SnO_2/NiO + h\upsilon \longrightarrow Ag\,(h^+)\,/SnO_2(e^-)\,/NiO$$
$$H_2O + 2h^+ \longrightarrow 1/2\,O_2 + 2H^+$$
$$HCrO_4^- + 7H^+ + 3e^- \longrightarrow Cr\,(III) + 4H_2O$$

However, in the photo reduction of Cr(VI) by our method, no precipitation of the sediment is obtained at pH 2.0. Hence, to confirm the presence Cr(III) in the sediment after the photo-reduction process, the pH of the solution is increased by addition of base, and it is observed that the sediment is precipitated out in the form of $Cr(OH)_3$. To prove this, the sediment is placed into a furnace for heating at 400 ºC for 1 h in air. The XRD pattern of the heated (400 ºC) sample shows (Fig. S14) the main characteristic peaks of chromic oxide (Cr_2O_3), because $Cr(OH)_3$ can be transformed into Cr_2O_3 when heating at high temperature.[73]

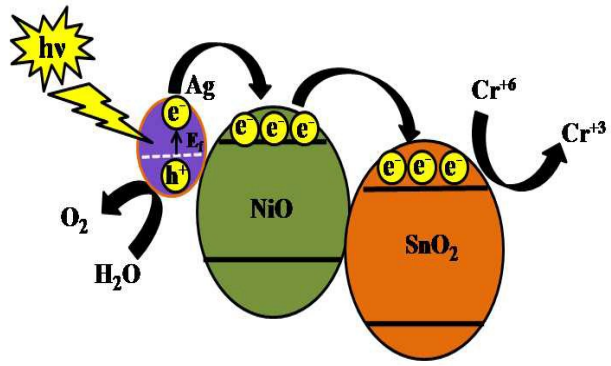

Fig. 13 Photocatalytic mechanism for the reduction of Cr(VI) by $Ag/SnO_2/NiO$ nanohybrid under visible light.

Conclusions

In summary, porous SnO_2/NiO heteronanostructure has been successfully fabricated by facile calcinations of a novel mixed-metal Sn-Ni NCP precursor. The prepared material is further successfully attached with metallic Ag nanoparticle by reduction of Ag^+ by UV irradiation, to obtain the $Ag/SnO_2/NiO$ nanohybrid. The novel $Ag/SnO_2/NiO$ has been successfully characterized and also has been applied for photocatalytic applications for the first time. The TEM images reveal spherical morphology of the Ag nanoparticles with average particle size of 15 nm, and hexagonal shaped SnO_2 and NiO with average particle size of 10 nm and 5 nm, respectively in the $Ag/SnO_2/NiO$ hybrid. The lower intensity PL spectrum confirms the inhibition of the electron–hole recombination and facilitation of more charge separation making the $Ag/SnO_2/NiO$ material more effective for photocatalytic reduction of toxic aqueous Cr(VI) under the visible light. It is observed that the $Ag/SnO_2/NiO$ exhibits much higher photoreduction capability (98% reduction in 60 min at pH 2.0 with 1 g/L catalyst) than individual SnO_2 and NiO or Ag/SnO_2 due to higher surface area, large pore volume and effective charge separation. In particular, the interfacial electron transfer from the NiO to SnO_2 in the hybrid could be feature prevents the recombination of charges, whereas the same is not possible for the individual SnO_2 and NiO or Ag/SnO_2. Therefore, heterostructured $Ag/SnO_2/NiO$ behaves superior in the enhanced photoreduction of Cr(VI) than the individuals metal oxides. The photocatalytic reduction of Cr(VI) in low pH condition is much higher than the solution of higher pH because at higher pH, the negatively surface of the catalyst repels the $Cr_2O_7^{2-}$ ion and also due to the deposition of $Cr(OH)_3$ on the surface of photocatalyst. Furthermore, the high photostability of the $Ag/SnO_2/NiO$ up to five repeated runs and less photo-corrosion signifies its potential for various applications, including the wastewater treatment.

Acknowledgements

The author, MR, thank the CSIR for research fellowship. Further, the authors extend their acknowledgements to CRF-IITKGP for TEM, HRTEM, FESEM, EDX analysis. The authors also acknowledge the DST-FIST funded XPS facility at the Department of Physics and Meteorology, IIT Kharagpur and SRIC IIT Kharagpur for SDGRI project (code: NPA).

References

1. N. H. Hsu, S. L. Wang, Y. C. Lin, G. D. Sheng and J. F. Lee, *Environ. Sci. Technol.,* 2009, **43**, 8801–8806
2. a) N. Kannan, A. Rajakumar and G. Rengasamy, *Environ. Technol.,* 2004, **25**, 513-522; b) N. Kannan and A. Rajakumar, *Indian J. Environ. Protect.,* 2009, 29, 533-538.
3. R. Aravindhan, B. Madhan, J. R. Rao, B. U. Nair and T. Ramsami, *Environ. Sci. Technol*., 2004, **38**, 300–306.
4. Y. Wang, B. Zou, T. Gao, X. Wu, S. Loua and S. Zhou*, J. Mater. Chem.,* 2012, **22**, 9034–9040.
5. A. K. Meena, K. Kadirvelu, G. K. Mishra, C. Rajagopal and P. N. Nagar, *J. Hazard. Mater*., 2008, **150**, 604–611.
6. H. Gu, S. B. Rapole, Y. Huang, D. Cao, Z. Luo, S. Wei and Z. Guo, *J. Mater. Chem. A,* 2013, **1**, 2011–2021.
7. P. O'Brien and A. Kortenkamp, *Transition Met. Chem.,* 1995, **20**, 636.
8. a) Z. G. ke, , Q. Huang, H. Zhang, and Z. L.Yu, *Environ. Sci. Technol.,* 2011, **45**, 7841−7847; b) X. Guo, G. T. Fei, H. Su and L. D. Zhang, *J. Phys. Chem. C,* 2011, **115**, 1608−1613.
9. J. J. Testa, M. A. Grela and M. I. Litter, *Environ. Sci. Technol*., 2004, **38**, 1589−1594.
10. D. W. Blowes, C. J. Ptacek and J. L. Jambor, *Environ. Sci. Technol.,* 1997, **31**, 3348−3357.
11. B. Gu and J. Chen, *Geochim. Cosmochim. Acta,* 2003, **67**, 3575−3582.
12. S. K. Li, X. Guo, , Y. Wang, F. Z Huang, Y. H. Shen, X. M. Wang and A. J. Xie, *Dalton Trans.,* 2011, **40**, 6745−6750.
13. Y. C. Zhang, J. Li and H. Y. Xu, *Appl. Catal. B,* 2012, **123**, 18−26.
14. D. Dinda, A. Gupta and S. K. Saha, *J. Mater. Chem. A,* 2013, **1**, 11221−11228.
15. S. G. Rashid, M. A. Gondal, A. Hameed, M. Aslam, M. A. Dastageer, Z. H. Yamani and D. H. Anjum, *RSC Adv.*, 2015, **5**, 32323.
16. U. Baig, R. A. K. Rao, A. A. Khan, M. M. Sanagi, M. A. Gondal, *Chem. Eng. J.*, 2015, **280**, 494–504.
17. L. Shen, S. Liang, W. Wu, R. Liang and L. Wu, *Dalton Trans.,* 2013, **42**, 13649−13657.
18. Z. He, Q. Cai, M. Wu, Y. Shi, H. Fang, L. Li, J. Chen and S. Song, *Ind. Eng. Chem. Res.,* 2013, **52**, 9556−9565.
19. Y. C. Zhang, L.Yao, G. Zhang, D. D. Dionysiou, J. Li and X. Du, *Appl. Catal. B,* 2014, **144**, 730−738.
20. J. Wang, X. Li, X. Li, J. Zhu and H. Li, *Nanoscale,* 2013, **5**, 1876.
21. Y. Qu, W. Zhou, L. Jiang and H. Fu, *RSC Adv,*. 2013, **3**, 18305–18310.
22. G. Dong and L. Zhang, *J. Phys. Chem. C,* 2013, **117**, 4062– 4068.
23. N. S. Waldmann and Y. Paz, *J. Phys. Chem. C,* 2010, **114**, 18946–18952.
24. H. Chen, C. E. Nanayakkara and V. H. Grassian, *Chem. Rev.,* 2012, **112**, 5919–5948.
25. S. A. Ansari, M. M. Khan, M. Omaish, J. Lee and M. H. Cho, *New J. Chem.,* 2014, **38**, 2462–2469.
26. M. Rakibuddin and R. Ananthakrishnan, *Photochem. Photobiol. Sci.*, 2015, DOI: 10.1039/C5PP00305A.
27. H. Ding, J. Zhu, J. Jiang, R. Ding, Y. Feng, G. Wei and X. Huang, *RSC Adv.,*. 2012, **2**, 10324–10329.
28. a) C. M. Fan, Y. Peng, Q. Zhu, L. Lin, R. X. Wang and A. W. Xu, *J. Phys. Chem. C,* 2013, **117**, 24157–24166; b) . H. C. Chiu and C. S. Y, *J. Phys. Chem. C,* 2007, **111**, 7256.
29. A. Subrahmanyam, A. Rajakumar, Md. Rakibuddin, T. P. Ramesh, M. R. Kiran, D. Shankari and K. Chandrasekhar, *Phys. Chem. Chem. Phys.*, 2014, 16, 24790—24799.
30. S. A. Ansari, M. M. Khan, M. O. Ansari, J. Lee and M. H. Cho, *RSC Adv.,* 2014, **4**, 26013.
31. Y. Tian and T. Tatsuma, *J. Am. Chem. Soc*., 2005, **127**, 7632.
32. M. A. Gondal, M. A. Dastageer, A. B. Khalil, S. G. Rashid and U. Baiga, *RSC Adv*., 2015, **5**, 51399.
33. J. Ran, J. Zhang, J. Yu, M. Jaroniec and S. Z. Qiao, *Chem. Soc. Rev*., 2014, **43**, 7787-7812.
34. Y.C. Liang, C. C. Wang, C. C. Kei, Y. C. Hsueh, W. H. Cho and T. P. Perng, *J. Phys. Chem. C,* 2011, **115**, 9498–9502.
35. D. H. Yu, X. Yu, C. Wang, X. C. Liu and Y. Xing, *ACS Appl. Mater. Interfaces*, 2012, **4**, 2781.

36. J. Song, H. Kim, Y. Jang and J. Jang, *ACS Appl. Mater. Interfaces*, 2013, **5**, 11563.
37. T. Hirakawa and P. V. Kamat, *J. Am. Chem. Soc.,* 2005, **127**, 3928.
38. M. Rakibuddin and R. Ananthakrishnan, *RSC Adv*., 2015, **5**, 68117.
39. L. Hu, P. Zhang, Y. Sun, S. Bao and Q. Chen, *ChemPhysChem,* 2013, **14**, 3953 – 3959.
40. C. Hua, X. Fang, Z. Wang and L. Chen, *Chem. Eur. J.,* 2014, **20**, 5487.
41. M. F. Hassan, M. M. Rahman, Z. Guo, Z. Chenc and H. Liua, *J. Mater. Chem.,* 2010, **20**, 9707–9712.
42. H. Ding, J. Zhu, J. Jiang, R. Ding, Y. Feng, G. Wei and X. Huang, *RSC Adv.,* 2012, **2**, 10324–10329.
43. Z. Wang, Z. Li, J. Sun, H. Zhang,W. Wang, W. Zheng and C. Wang, *J. Phys. Chem. C,* 2010, **114**, 6100–6105.
44. L. Wang, J. Deng, T. Fei and T. Zhang, *Sensor. Actuat. B,* 2012, **164**, 90– 95.
45. M. Rakibuddin and R. Ananthakrishnan, *Appl. Surf. Sci.*, 2016, **362**, 265-273.
46. E. S. Bárdos, H. Czili, A. Horváth*, J. Photochem. Photobiol. A: Chem.,* 2003, 154, 195–201.
47. G. E. Patil, D. D. Kajale, V. B. Gaikwad and G. H. Jain*, Int. Nano Lett..*, 2012, **2**, 17–21.
48. H. Guan, C. Shao, S. Wen, B. Chen, J. Gong and X. Yang, *Inorg. Chem. Commun.,* 2003, **6**, 1302.
49. J. Ma, J. Zhang, Z. Xiong, Y. Yong and X. S. Zhao, *J. Mater. Chem*., 2011, **21**, 3350.
50. Z. Zhang, C. Shao, X. Li, C. Wang, M. Zhang, and Y. Liu*, ACS Appl. Mater. Interfaces,* 2010, **2**, 2915-2923.
51. S. Balachandran, K. Selvam, B. Babub and M. Swaminathan, *Dalton Trans.,* 2013, **42**, 16365.
52. B. R. Jayan and A. Manthiram, *RSC Adv.,* 2013, **3**, 5412.
53. H. Zhang, G. Wang, D. Chen, X. J. Lu and J. H. Li, *Chem. Mater*., 2008, **20**, 6543.
54. Y. Zhan, C. Yin, C. Zheng, W. Wang and G. Wang, *J. Solid State Chem*., 2004, **177**, 2281.
55. A. Mansour, *Surf. Sci. Spectra*, 1994, **3**, 231.
56. A. R. G. Elipe, J. P. Holgado, R. Alvarez and G. Munuera*, J. Phys. Chem*., 1992, **96**, 3080.
57. Y. Chen, K. Munechika and D. S. Ginger *Nano Lett*., 2007, **7**, 690-696.
58. Y. Z. Li, H. Zhang, Z. M. Guo, J. J. Han, X. J. Zhao, Q. N. Zhao and S. J. Kim, *Langmuir,* 2008, **24**, 8351
59. M. Shirzad Siboni , M.T. Samadi , J.K. Yang & S.M. Lee, *Environ. Technol.*, 2011, **32,** 1573-1579
60. X. Liu, L. Pan, T. Lv, T. Lu, G. Zhu, Z. Sun and C. Sun, *Catal. Sci. Technol.*, 2011, **1**, 1189–1193.
61. D. Zhang, X. Li, H. Tan, G. Zhang, Z. Zhao, H. Shi, L. Zhang, W. Yu and Z. Sun, *RSC Adv.,* 2014, **4**, 44322–44326.
62. L. Mao, J. Li, Y. Xie, Y. Zhong, and Y. Hu, *RSC Adv.,* 2014, **4**, 29698–29701.
63. Y. Du, Z. Tao, J. Guan, Z. Sun, W. Zeng, P. Wen, K. Ni, J. Ye, S. Yang, P. Du and Y. Zhu*, RSC Adv*., 2015, DOI:10.1039/C5RA15561D.
64. J. Yu,. S. Zhuang, X. Xu, W. Zhu, B. Feng and J. Hu, *J. Mater. Chem. A,* 2015, **3**, 1199–1207.
65. L. Shang, B. Li, W. Dong, B. Chen, C. Li, W. Tang, G. Wang, J. Wu, Y. Ying*, J. Hazard. Mater.,* 2010, **178**, 1109–1114.
66. W. Dong, Y. Zhu, H. Huang, L. Jiang, H. Zhu, C. Li, B. Chen, Z. Shib and G. Wang, *J. Mater. Chem. A*, 2013, **1**,10030.
67. J. Wang, X. Li, X. Li, J. Zhu and H. Li, *Nanoscale,* 2013, **5**, 1876−1881.
68. D. K. Padhi and K. Parida. *J. Mater. Chem. A*, 2014, **2**,10300-10312.
69. C. Mondal, M. Ganguly, J. Pal, A. Roy, J. Jana and T. Pal, *Langmuir,* 2014, **30**, 4157−4164.
70. C. M. Welch, O. Nekrassova and R. G. Compton, *Talanta*, 2005, **65**, 74–80.
71. Z. Ke, Q. Huang, H. Zhang and Z. Yu, *Environ. Sci. Technol*., 2011, **45**, 7841–7847.
72. Z. Khan, M. Khannam, N. Vinothkumar, M. Deb and M. Qureshi, *J. Mater. Chem*., 2012, **22**, 12090.
73. P. Ratnasamy and A. J. Leonard, *J. Phys. Chem.* 1972, **76**, 1838–1843.

Graphical Abstract:

Novel Ag deposited Nano Coordination Polymers Derived Porous SnO_2/NiO Heteronanostructure for Enhanced Photocatalytic Reduction of Cr (VI) under Visible Light

Md. Rakibuddin and Rajakumar Ananthakrishnan*

Department of Chemistry, Green Environmental Materials and Analytical Chemistry Laboratory, Indian Institute of Technology, Kharagpur 721 302, India.

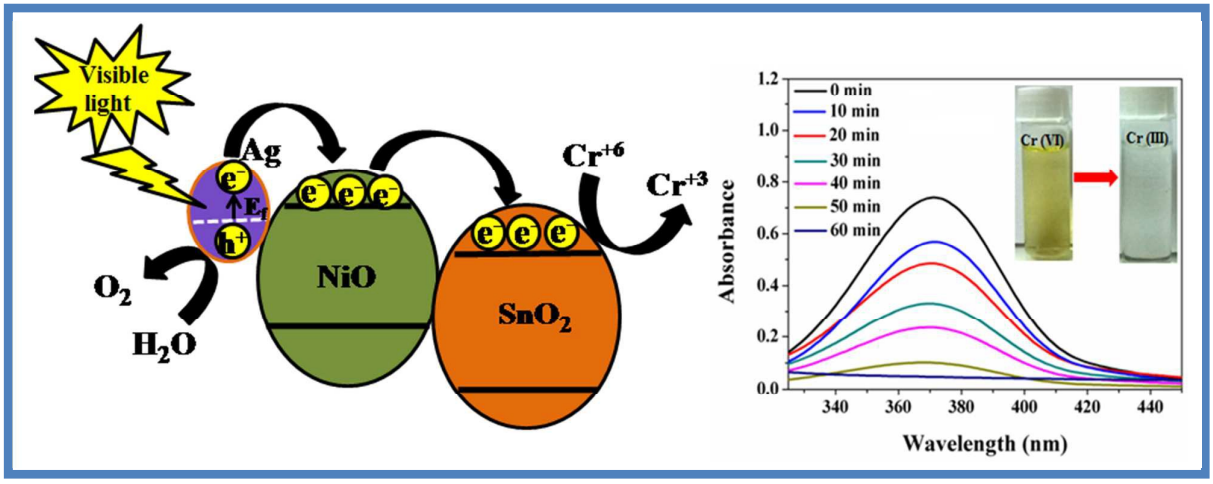

A novel silver deposited SnO_2/NiO heteronanostructure is prepared and applied for photocatalytic reduction of toxic aqueous Cr (VI) under visible light condition.